Available online at www.sciencedirect.com
ScienceDirect
Journal of Power Sources 164 (2007) 519–526
JOURNAL OF POWER SOURCES
www.elsevier.com/locate/jpowsour

Spatially electrodeposited platinum in polyaniline doped with poly(styrene sulfonic acid) for methanol oxidation

Li-Ming Huang, Wang-Rung Tang, Ten-Chin Wen *

Department of Chemical Engineering, National Cheng Kung University, Tainan 70101, Taiwan

Received 16 October 2006; received in revised form 23 November 2006; accepted 23 November 2006
Available online 2 January 2007

Abstract

Polyaniline (PANI) can be doped with poly(styrene sulfonic acid) (PSS) via doping–dedoping–redoping process. The specific characteristics of PANI doped with PSS (PANI-PSS) were checked by UV–vis spectroscopy, cyclic voltammetry, scanning electron microscopy (SEM) and X-ray photoelectron spectroscopy (XPS). PANI-PSS was found to have spatial structure with minimum degradation products. Platinum can be potentiostatically deposited in a spatial layer of the PANI-PSS as evidenced by electron dispersive element analysis (EDS) and Auger electron spectroscopy (AES). The electrochemical measurements demonstrated that PANI-PSS-Pt exhibited a much higher electrocatalytic activity for methanol oxidation than PANI-Pt.

Keywords: Polyaniline; Poly(styrene sulfonic acid); Pt particles; AES; Methanol oxidation

1. Introduction

Fuel cells are attractive sources of electrical power since they realize the direct conversion of chemical to electrical energy. One promising system is the direct methanol fuel cell (DMFC) [1–3]. Unfortunately, the expensive catalytic materials, such as platinum, and relatively low electrocatalytic efficiency for electrochemical reactions of the fuel are drawbacks. To date, efforts have focused on the development if techniques of produce Pt catalysts with a high surface area [4,5]. It has been proved that the support materials in electrocatalysts play an important role to the electrochemical performance [6]. Though improvement has been made in the catalytic activity and stability of the electrocatalyst by effectively dispersing Pt particles onto the electrically conducting supports, many efforts are still continuing.

In fact, the choice of a suitable supporting material is an important factor that may affect the performance of supported electrocatalysts owing to interactions and surface reactivity [7,8]. Pt supports can be separated as two categories. One is carbon supported, including traditional carbon support materials (XC-72), graphite nanofibers (GNFs) [9,10], carbon nanotubes [11,12] and mesocarbon microbeads (MCMB) [13,14]. However, the limitation of carbon in terms of performance is that the proton does not easily contact with catalyst. The other group is the conducting polymers, such as polyaniline (PANI) [15,16], and polypyrrole (PPY) [17,18]. Conducting polymer-stabilized metal nanoparticles or nanoclusters often act as an excellent homogeneous catalyst and show interesting properties [19–21]. They not only provide access to a large number of catalytic sites but also offer the possibility of synergetic effect between the polymer matrix and the metal nanoparticles. Another advantage of the polymer matrix might provide an efficient pathway for electron and preferably for protonic species for DMFC application.

Recently, new attempts have been focused on the modification of conducing supports with increasing Pt utilization and enhancing the electrocatalytic properties toward methanol oxidation. Peng and co-workers [8] reported that highly dispersed Pt nanoparticles supported in sulfonated carbon nanotubes (Pt/sulfonated-CNTs) with high electrocatalytic activity for DMFC. Huguenin and co-workers [22] showed a biodegradable chitosan and poly(vinyl sulfonic acid) (PVS) in layer-by-layer (LB) film serving as templates to yield metallic platinum. Bensebaa et al. [23] synthesized polypyrrole di(2-ethylhexyl) sulfosuccinate (PPYDEHS) stabilized PtRu catalysts for DMFC. Dong and co-workers [24] synthesized a stable

* Corresponding author. Tel.: +886 6 2385487; fax: +886 6 2344496.
E-mail address: tcwen@mail.ncku.edu.tw (T.-C. Wen).

0378-7753/$ – see front matter © 2006 Elsevier B.V. All rights reserved.
doi:10.1016/j.jpowsour.2006.11.082

electroactive conducting copolymer film of poly(aniline-*co*-*o*-aminobenzensulfonic acid) three-dimensional tubal networks on indium oxide glass (ITO) and the cytochrome *c* was immobilized on the matrix by the electrostatic interactions. The composite film showed direct electron transfer between protein and electrode surface with high electron transfer rate of 12.9 s.

Modification of electrode surfaces provides an attractive way of confining catalytic species to the effective spatial region and combines the experimental advantages of heterogeneous catalysts with the benefits of a three-dimensional distribution of active centers typically characteristic of homogeneous catalysts. Hence, the introduced sulfonic acid groups (SO_3H) might affect the properties of supporting materials and performance for its application in DMFC. This motivated us to investigate the feasibility of incorporating SO_3H groups into conducting polymer as support for Pt. We employed a simple "doping–dedoping–redoping" method to introduce the SO_3H groups (poly(styrene sulfonic acid), PSS) into PANI in the present study. PANI-PSS composite behaves as a good probe for the deposition Pt particles and increased the density of the active sites in the polymer film. The well-dispersed Pt particles inside such conducting composite support can lead to good Pt utilization and an improvement of the catalytic activity for methanol oxidation. In the work, we describe the synthesis and characterization of PANI-PSS composite film incorporated PSS into PANI matrix via doping–dedoping–redoping method. PANI-PSS composite film embedded Pt particles by electrodeposition technique shows higher electrocatalytic properties and stability for methanol oxidation than that of Pt deposited in PANI without PSS incorporated and is more promising for application in electrocatalyst.

2. Experimental

2.1. Preparation of PANI-PSS and PANI-PSS-Pt composite films

PANI film was prepared by the electrochemical polymerization (at a constant potential of 0.8 V) of aniline (Merck) in 0.5 M H_2SO_4 aqueous solution as described elsewhere [25]. Emeraldine base form (EB) of PANI was obtained by treating the PANI film in ammonium hydroxide (Aldrich), and then the EB film was redoped by poly(styrene sulfonic acid) (PSS) (M_w = 75,000, Aldrich). PANI doped with PSS is denoted as PANI-PSS.

Pt particles were deposited onto the ITO/PANI-PSS from a solution of H_2PtCl_6. For a comparative purpose, Pt particles were deposited onto PANI matrix under otherwise similar conditions to the deposition of Pt particles onto ITO/PANI-PSS. Typically, a plating solution consisting of 5 mM $H_2PtCl_6{\cdot}6H_2O$, 0.01 M HCl, and 0.1 M KCl was used. The reduction of Pt particles was accomplished at −0.2 V for the charge passed of 0.1 C. After Pt particles incorporation, the electrodes were rinsed with double distilled water for 5 min then dried at 100 °C for 3 min. Pt electrodeposited in PANI and PANI-PSS denoted as PANI-Pt and PANI-PSS-Pt.

2.2. Physical and electrochemical characterizations

The surface morphologies of PANI-PSS and PANI-PSS-Pt were observed with a scanning electron microscopy (Philips X1-40 FEG). The X-ray photoelectron spectroscopy (XPS) measurement was performed with ESCA210 and MICROLAB 310 D (VG Scientific Ltd., U.K.) spectrometers. XPS spectra were recorded with Mg Kα($h\nu$ = 1256.6 eV) irradiation as photon source with a primary tension of 12 kV and an emission center of 20 mA. The pressure of the analysis chamber scans was kept approximately at 10^{-10} mbar during the scan. Auger electron spectroscopy (AES) depth profiles were performed with Microlab 310 D (VG Scientific Ltd.) spectrometer at an emission current of 0.1 and 8 mA with gun tension of 10 (electron) and 3 kV (ion), respectively.

Electrochemical characterizations of composite electrodes were performed using PGSTAT20 electrochemical analyzer, AUTOLAB Electrochemical Instrument (The Netherlands). All experiments were carried out in a three-component cell. An Ag/AgCl electrode (in 3 M KCl), Pt wire and composite electrode (1 cm^2 area) were used as reference, counter and working electrodes, respectively. A Luggin capillary, whose tip was set at a distance of 1–2 mm from the surface of the working electrode, was used to minimize errors due to *iR* drop in the electrolytes.

2.3. Methanol electrooxidation on PANI-PSS-Pt composite electrode

Methanol electrooxidation on PANI-Pt and PANI-PSS-Pt was examined by CV at 10 mV s^{-1} ranged from −0.2 to 1.0 V and potential–time curves at 0.02 mA cm^{-2} in 0.1 M CH_3OH + 0.5 M H_2SO_4 solution. All the electrochemical experiments were carried out at room temperature.

3. Results and discussion

3.1. Electrochemical characterization of PANI and PANI-PSS

The incorporation of PSS into PANI has been achieved by "doping–dedoping–redoping" process, being evidenced by UV–vis spectroscopy. Fig. 1 shows UV–vis spectra for PANI doped form (electrochemical polymerization of PANI in H_2SO_4 medium), dedoped form and redoped form with PSS. The doped form of PANI (doped with H_2SO_4, curve a) possesses three peaks at ca. 356, 434 and 780 nm (free carrier tail). These peaks correspond to electron transition from valance band to polaronic band characteristic of the doped emeraldine oxidation state of PANI [25]. Dipping the emeraldine salt of PANI with ammonium hydroxide yields the dedoped form of PANI. The corresponding UV–vis spectrum (curve b) exhibits two absorption maxima at 326 and 598 nm, representing the π–π^* transition and charge transfer excitation-like transition bands of the emeraldine base form of PANI [26]. After immersing the dedoped form of PANI in PSS solution, three characteristic peaks can be observed in UV–vis spectrum (curve c) and similar to that of the PANI doped form. It indicates that PANI can be doped with

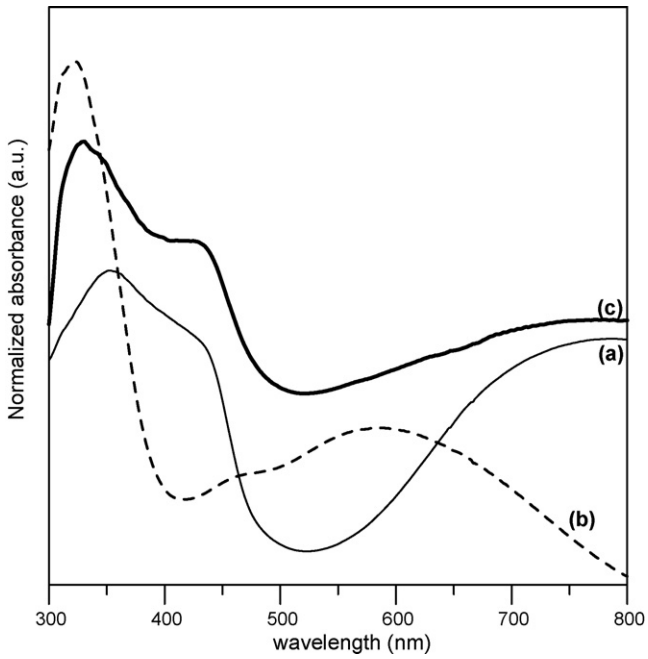

Fig. 1. UV–vis spectra of (a) PANI-H_2SO_4 (emeraldine salt), (b) emeraldine base (EB) and (c) redoped by PSS (PANI-PSS, emeraldine salt).

PSS (PANI-PSS) by the simple "doping–dedoping–redoping" technique.

Fig. 2 presents the CVs of PANI and PANI-PSS in 0.5 M H_2SO_4 solution. PANI and PANI-PSS show prominent redox peaks at around 0.3 V (peak A), 0.62 V (peak B) and higher than 0.8 V (peak C). Peaks A and C are assigned for the conversion of leucoemeraldine to emeraldine (peak A), emeraldine to pernigraniline (peak C). Peak B corresponds to the redox reaction of degradation products (hydroquinone to quinone) [27,28]. The differences in electrochemical properties between PANI and PANI-PSS can be seen from the comparative analysis of peak potential and current density at the redox sites. Peaks A–C for PANI-PSS appear at lower anodic peak potentials than those for PANI. This is attributed to the decrease in the resistance of the

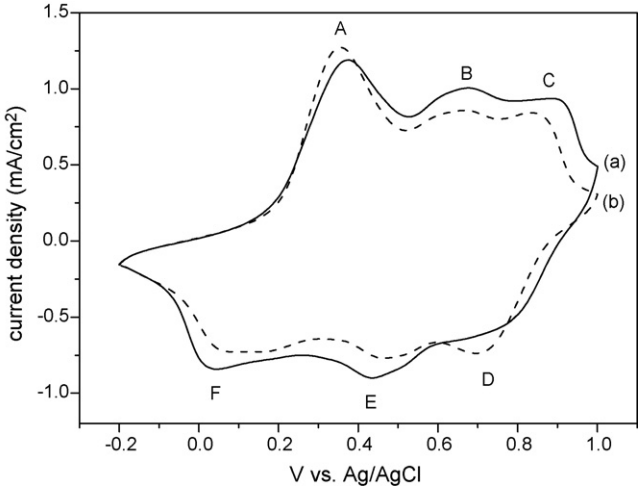

Fig. 2. Cyclic voltammograms of (a) PANI and (b) PANI-PSS in 0.5 M H_2SO_4 solution, scan rate = 50 mVs^{-1}.

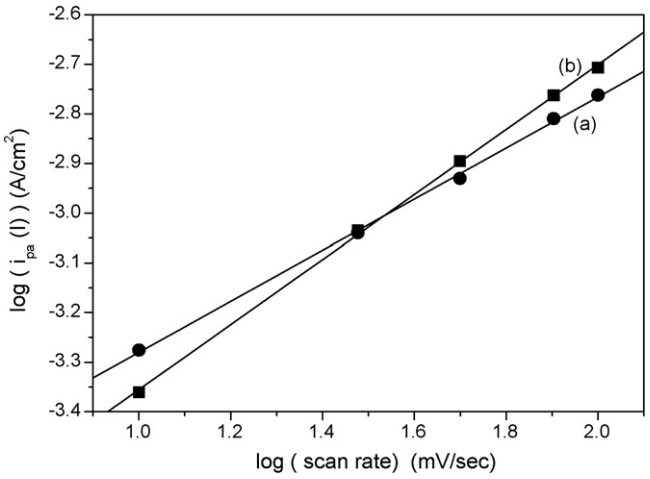

Fig. 3. Dependence of the peak current on the scan rate: (a) PANI and (b) PANI-PSS.

polymer film as a result of incorporation of PSS having SO_3H groups in PANI film. PSS incorporation in PANI film makes charge neutralization easy upon oxidation of PANI. Reports on other features are also available. Ding and Park [29] noticed a faster polymerization of ANI in PSS. Kang et al. [30] reported a relatively faster redox reaction at high pH values and better mechanical properties for PANI doped with PSS than PANI itself. Additionally, the current density at peak A is much higher for PANI-PSS than PANI. This indicates that conversion of PANI from leucoemeraldine to emeraldine is facile in PANI-PSS in comparison with PANI. From the above analysis of CVs of PANI and PANI-PSS, the incorporation of PSS in PANI might affect the charge transport during electrochemical reaction. To explain this, the double logarithmic plots between peak current (i_{pa}) versus scan rate (v) (Fig. 3) were made and found to be linear with different slope values. It is known that linearity for the plot between peak current and v would correspond to the surface bound transport process and a different type of linear for the plot of peak current versus $v^{1/2}$ would signify a diffusion control process [27]. The slope values of the double logarithmic plot were 0.52 and 0.66 for PANI and PANI-PSS, respectively. This suggests change in charge transport mechanism between PANI and PANI-PSS. While PANI may tend to have diffusion control transport processes, PANI-PSS may have surface bound transport processes.

3.2. Morphology

From the above discussion, it is conceivable that surface morphology of PANI is influenced by the incorporation of PSS into PANI structure. As revealed by the SEM photographs in Fig. 4, PANI (Fig. 4a) has grains with porous structure, whereas PANI-PSS (Fig. 4b) shows better cohesion with compact layer structure. The change in morphology of PANI-PSS in contrast to PANI arises from the influence of PSS molecules on the orientation of PANI to the ITO substrate. PSS acts as not only the dopant but also the bridge to connect the interchain of PANI to form the spatial network structure. This spatial network struc-

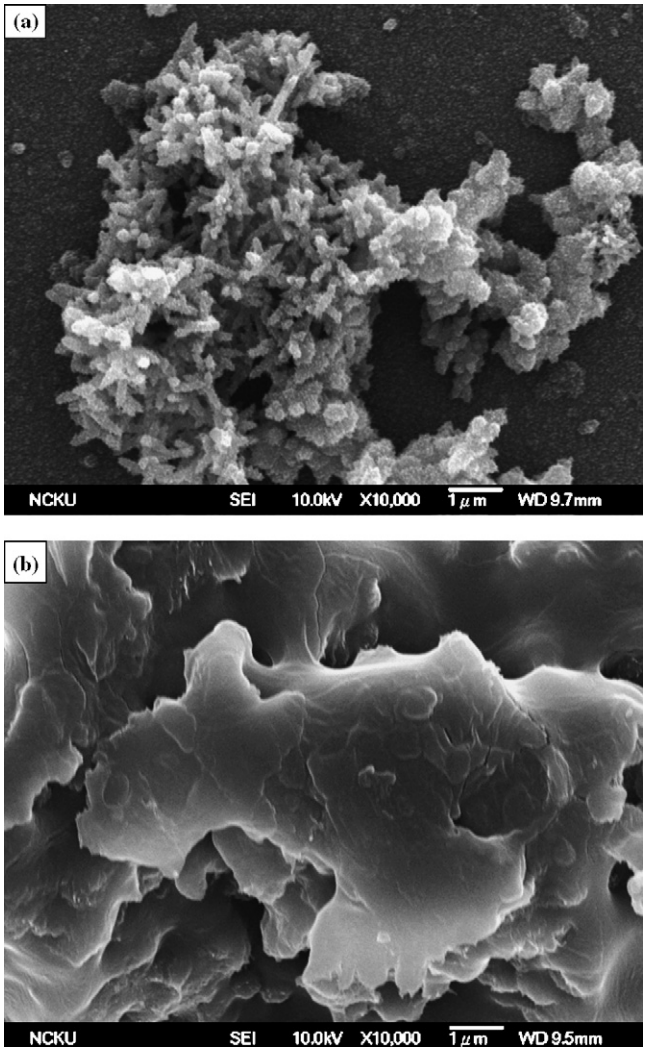

Fig. 4. SEM images of (a) PANI and (b) PANI-PSS composite.

ture of PANI-PSS might be valuable for the electrodeposition of Pt.

3.3. XPS analysis

To investigate the effect of PSS on the intrinsic structure of PANI, PANI and PAN-PSS were subjected to XPS examination. XPS spectra of core-level N_{1s} for PANI and PANI-PSS are shown in Fig. 5. Broad peaks in these core-level spectra imply the existence of several structures. Thus, XPS peaks were deconvoluted into Gaussian component peaks [31] at 398.3, 399.1, 400.0, 401.1 eV and 398.1, 399.3, 400.1 and 401.3 eV for PANI and PANI-PSS, respectively, which represented the −N=, −N−, $-N^+$ and $=N^+$. The area ratio of these four components was calculated and listed in Table 1. The ratio of [=N−]/[−NH−] provides a direct evaluation of the intrinsic oxidation state of PANI. Therefore, the ratio of 0.36 for PANI-PSS is lower than that (0.87) for PANI, suggesting that the intrinsic oxidation state of PANI-PSS is decreased due to the incorporation of PSS. This aspect was also evident from the CV result that the current density of peak C (Fig. 2) is the lower for PANI-PSS than PANI.

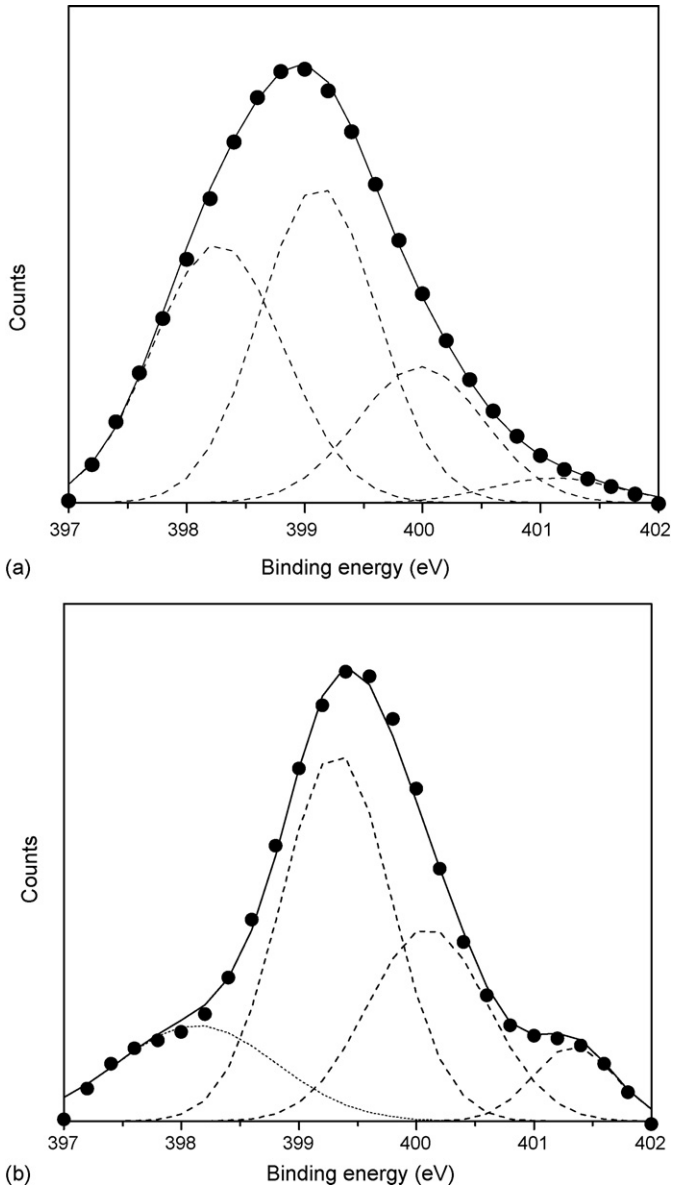

Fig. 5. N_{1s} core level spectra of (a) PANI and (b) PANI-PSS composite film.

The reason for low imine content of PANI-PSS might be due to the steric hindrance effect of SO_3H group and restricted the conversion of emeraldine to pernigraniline. The other important feature is the higher positive charge nitrogen (0.34%) in PANI-PSS than PANI (0.23%). This indicates that the easier doping for PANI-PSS than PANI is due to SO_3H groups in PSS. In XPS experiment, we also observed that the sulfur content (S/N = 0.89) is much higher in PANI-PSS than PANI (S/N = 0.25). The excess SO_3H groups in PANI-PSS play an addition role for the further

Table 1
Influence of the incorporated PSS on the oxidation state, doping degree and defect density of the PANI films

Sample	[=N/−NH−]	$[N^+ + =N^+/N]$	[C=O/C]	[C−O/C]
PANI	0.87	0.23	0.07	0.14
PANI-PSS	0.36	0.34	0.02	0.02

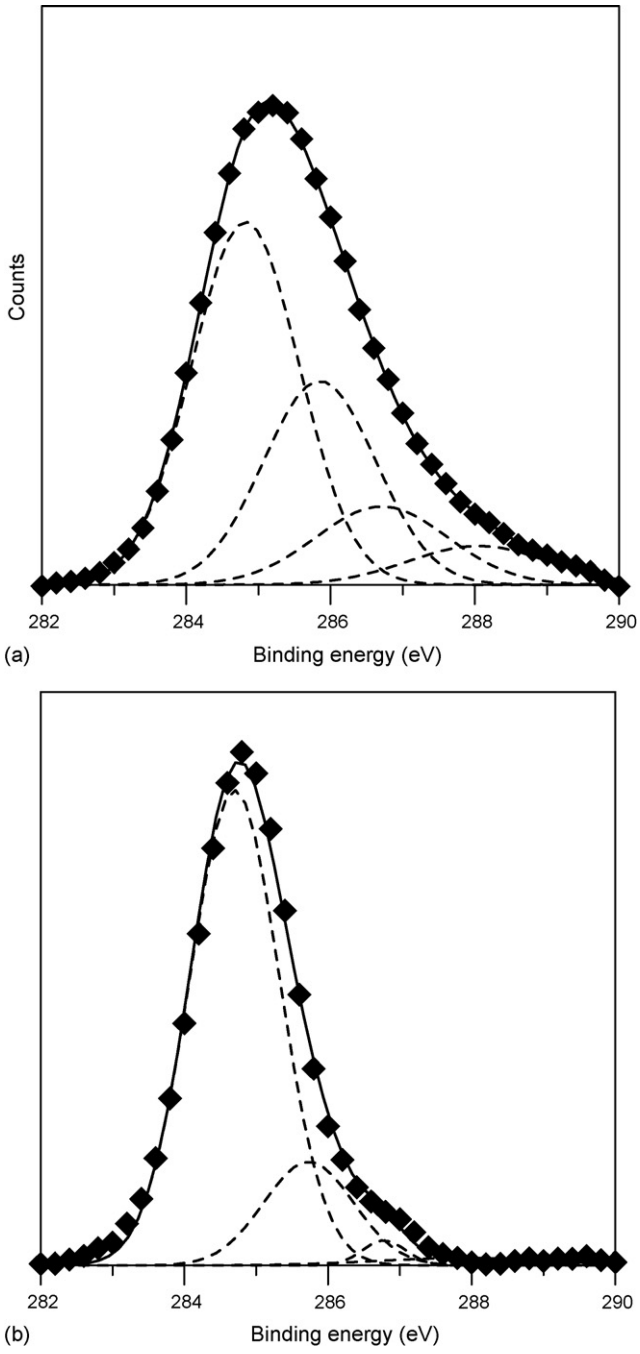

Fig. 6. C_{1s} core level spectra of (a) PANI and (b) PANI-PSS composite film.

deposition of Pt and provide the path for proton migration in methanol oxidation.

Furthermore, XPS C_{1s} core-level spectra of PANI and PANI-PSS provide information for the existence of side products (hydroquinone and quinone) in the polymer matrixes. Fig. 6 shows XPS spectra of C_{1s} core-level for PANI and PANI-PSS. Through Gaussian–Lorentzian fitting, these C_{1s} spectra can be fitted into four components at 284.8 (C–C/C–H), 285.9 (C=N), 286.7 (C–O) and 288.1 eV (C=O), respectively. The highest binding energy is attributed to the presence of carbonyl carbons (C=) that are formed by the attack of water molecules during the electrochemical reaction [32]. Therefore, the relative area of these two higher peaks of binding energy is used to calculate the density of carbonyl defects within the polymers, showing the side products of the polymers [31]. From Table 1, the defect density (hydroquinone and quinone) gradually decreased with incorporating PSS into PANI. PANI doped with PSS is expected to twist up to form a spatial network structure (Fig. 4b). The steric effect of PSS in spatial network structure of PANI-PSS decelerates the degradation of PANI to hydroquinone/quinone, resulting the lower portion of the side products for PANI-PSS than PANI. Meanwhile, XPS analysis shows that PANI-PSS has the higher doping degree and lower defect density than PANI, which probably results better electrochemical properties for the electrodeposition of Pt and the enhancement of methanol oxidation.

3.4. Growth of platinum into PANI and PANI-PSS

In this study, platinum was electrodeposited into PANI and PANI-PSS at constant potential (−0.2 V versus Ag/AgCl) with the same charge of 0.1 C. It can be seen from SEM photographs, morphologies of PANI and PANI-PSS did not change much with the electrodeposited Pt. An examination of Fig. 7(a and b) reveals that there are particles in PANI surface (Fig. 7a) while the same spatial structure in PANI-PSS surface (Fig. 7b). We anticipated that Pt particles are embedded in PANI-PSS spatial network structure. The insets in Fig. 7 show EDS results of Pt in PANI and PANI-PSS. The bright spots of Pt represent the existence of platinum in PANI and PANI-PSS (denoted as PANI-Pt and PANI-PSS-Pt).

The Pt and S depth profiles of PANI-Pt and PANI-PSS-Pt are shown in Fig. 8. Pt reaches the maximum at 440 s and then decreases to a shoulder between 1240 and 1940 s for PANI-Pt (Fig. 8a). Afterwards, it decreased sharply between 1940 and 2340 s. From this curve, Pt is enriched on the surface of PANI matrix although Pt particles are deposited in PANI matrix. In contrast to PANI-Pt, Pt reaches the maximum at 100 s, and then a broad peak is located between 200 and 1500 s for PANI-PSS-Pt (Fig. 8b). It implies that Pt is dispersed uniformly into PANI-PSS spatial network structure. To deposit Pt into pre-synthesized PANI matrix, proper electrodeposition method should be used. The theoretical potential of $[PtCl_6]^{2-}$ reduction ($Pt^{4+} \rightarrow Pt^0$) is approximately 0.5 V, whereas the cathodic peak current of Pt deposition appears at more negative potentials around −0.2 V (versus Ag/AgCl). This may be ascribed to a kinetic hindrance of the $[PtCl_6]^{2-}$ reduction in the interior of PANI film [33]. Under this negative potential applied, the structural characteristic of PANI is transformed into insulating state (leucoemeraldine) with increasing the charge transfer resistance. Meanwhile, SO_4^{2-} and $PtCl_6^{2-}$ will be driven out from the polymer matrix to the bulk electrolyte. Consequently, the nucleation of Pt spontaneously occurred at PANI surface. The above discussion and hypothesis can be validated by Fig. 8a, showing the enrichment of Pt near the surface of PANI and decreasing trend in sulfur (SO_4^{2-}). The enrichment of Pt near the surface of PANI is consistent with the spherical Pt particles on PANI surface from the morphology of PANI-Pt (Fig. 7a). In contrast to PANI-Pt, PANI doped with PSS will twist up to form a spatial network struc-

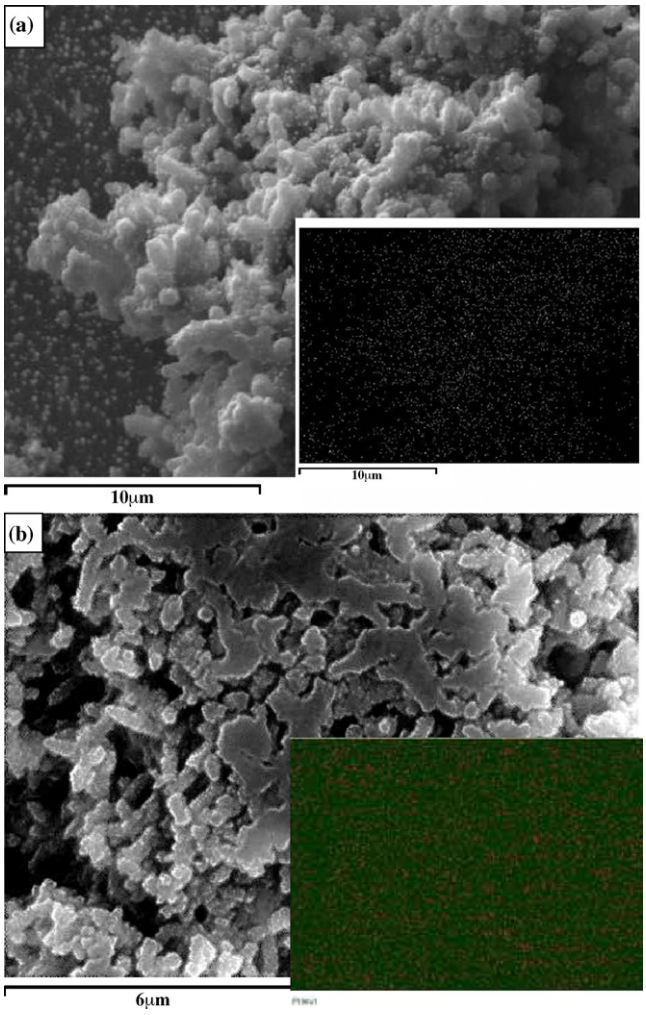

Fig. 7. SEM images of (a) PANI-Pt and (b) PANI-PSS-Pt. Inset: X-ray maps show bright spots for Pt.

ture. Under the applied negative potential, SO_3H ions would not be driven out from PANI-PSS matrix due to SO_3H groups pending on PSS polymer chain. Fig. 8b exhibits a plateau of sulfur content between 200 and 1500 s in PANI-PSS-Pt, indicating that a spatial network structure of PANI-PSS can hold SO_3H groups in PANI at the negative potential (−0.2 V). The existence of SO_3H groups in PANI-PSS assists holding $[PtCl_6]^{2-}$ ions in polymer matrix by the interaction of Pt^{4+} ions with SO_3H groups even though under the negative potential. As the negative potential applied, the nuclei of Pt are immediately generated around the SO_3H groups, resulting the homogenous distribution of Pt in PANI-PSS spatial network structure evidenced by Fig. 8b. The homogenous distribution of Pt in PANI-PSS spatial network structure might increase the utilization of Pt for methanol oxidation.

3.5. Electrocatalytic activity and stability of PANI-PSS-Pt for methanol oxidation

To evaluate the performance of PANI-Pt and PANI-PSS-Pt in the electrooxidation of methanol, cyclic voltammograms (CVs) were recorded in 0.1 M CH_3OH + 0.5 M H_2SO_4 solution. For

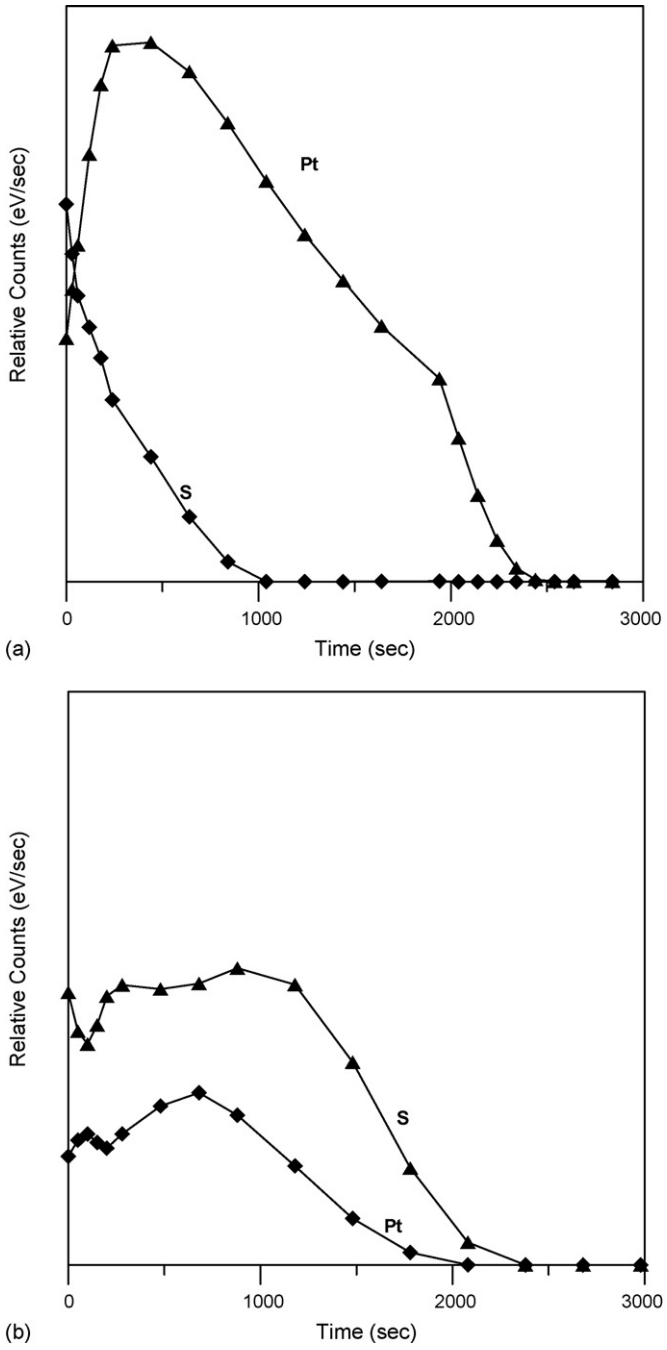

Fig. 8. AES depth profiles of (a) PANI-Pt and (b) PANI-PSS-Pt. (▲) sulfur and (♦) platinum signals.

comparative purpose, CVs were also collected in 0.5 M H_2SO_4 (Fig. 9, inset) for corresponding electrochemical characteristics, before methanol oxidation was undertaken. The CVs for both PANI-Pt and PANI-PSS-Pt are similar to those for the PANI and PANI-PSS in 0.5 M H_2SO_4 solution. Three well-defined redox pairs can be seen due to the conversion of leucoemeraldine to emeraldine (0.3 V), emeraldine to pernigraniline (0.8 V) and hydroquinone to quinone (0.5 V). It is worth to note that the response corresponding to hydrogen adsorption/desorption appears in the potential range between −0.2 and 0.0 V. It is known that the charge passed for H-adsorption (Q_H) represents

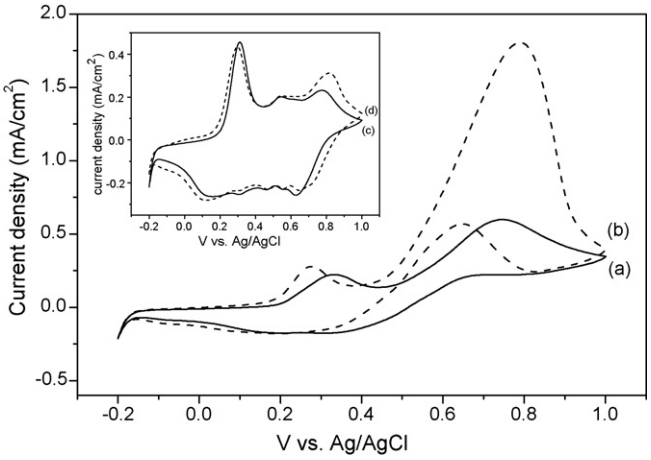

Fig. 9. Cyclic voltammograms of (a) PANI-Pt and (b) PANI-PSS-Pt in 0.1 M $CH_3OH + 0.5$ M H_2SO_4 solution, scan rate = 10 mV s^{-1}. Inset: cyclic voltammograms of (c) PANI-Pt and (d) PANI-PSS-Pt in 0.5 M H_2SO_4 solution, scan rate = 10 mV s^{-1}.

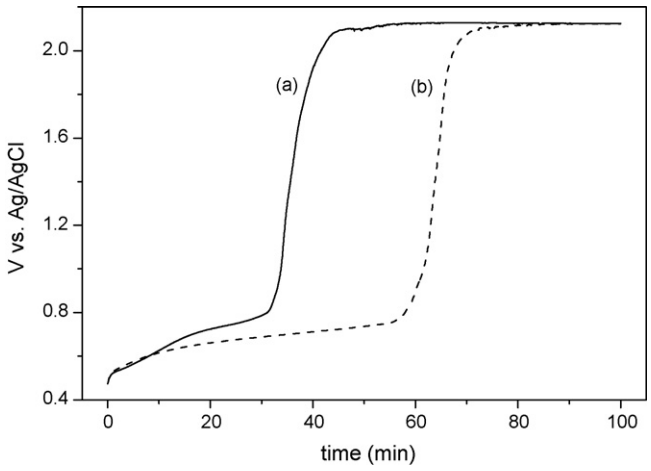

Fig. 10. Potential–time of (a) PANI-Pt and (b) PANI-PSS-Pt in 0.1 M $CH_3OH + 0.5$ M H_2SO_4 solution at 0.02 mA cm^{-2}.

the number of sites of Pt available for hydrogen adsorption and desorption [34,35]. The charge for hydrogen adsorption for PANI-PSS-Pt was 2.13 mC cm^{-2}, which is 1.60 times larger than that for PANI-Pt (1.33 mC cm^{-2}). It implies that PANI-PSS-Pt owns higher surface area of Pt than PANI-Pt, being attributable to the homogeneous dispersion of Pt in PANI-PSS spatial network structure.

The electrocatalytic activity of PANI-Pt and PANI-PSS-Pt toward methanol oxidation is shown in Fig. 9. Methanol oxidation commenced at about 0.4 V, giving a peak at about 0.75 V. On the reverse-going scan, an oxidation peak occurred at about 0.65 V, and no reduction peak was observed. This kind of anomalous behavior was attributed to the adsorption and interaction of various intermediate species at the electrode surface [36,37]. The onset potential for methanol oxidation is 0.44 and 0.38 V for PANI-Pt and PANI-PSS-Pt, respectively. The lowing onset potential of PANI-PSS-Pt is attributed to SO_3H in PANI-PSS that can shuttle the electrons easily (high positive charge nitrogen content) and provide the pathway for proton migration (homogenous distributed PSS, Fig. 8b) toward methanol oxidation. Based on the peak current at ca. 0.75 V, the oxidation current densities for methanol oxidation are about 0.6 and 1.81 mA cm^{-2} for PANI-Pt and PANI-PSS-Pt, respectively. The reasons for the improvement of catalytic activity of Pt embedded in PANI-PSS are presented here.

Firstly, PANI doped with PSS can twist up to form a spatial network structure. The uniform dispersion of Pt in PANI-PSS can be achieved and enhance Pt utilization efficiency for methanol oxidation. Secondly, we anticipated that SO_3H in PANI-PSS may act as a stabilizer for Pt particles and prevent aggregation of Pt particles. The steric and electrostatic stabilization of Pt particles might be achieved by PANI-PSS. The above view is supported by the following reports [38,39]. Dalmia et al. [38] reported the feasibility of synthesizing nanometer-sized Pt colloids using a negatively charge polymer, poly(*N*-sulfonatopropyl *p*-benzamide). Ahmadi et al. [39] demonstrated the synthesis of nanometer-size Pt colloids using polyacrylic acid and the effect of the polymer concentration on the shape of Pt particle. Thirdly, according to the above results from CV and XPS analysis of PANI and PANI-PSS, the minimum existence of side products (hydroquinone and quinone) in PANI-PSS contributes to enhance methanol oxidation on PANI-PSS-Pt composite.

The utilization efficiency of Pt toward methanol oxidation is limited by CO poison on Pt surface. The stability and CO poison effect on PANI-Pt and PANI-PSS-Pt can be evaluated from the chronopotentiometric response of PANI-Pt and PANI-PSS-Pt in 0.1 M $CH_3OH + 0.5$ M H_2SO_4 as shown in Fig. 10. Generally, the driving voltage will increase when CO adsorbed on Pt surface in order to maintain the same electrocatalytic properties of Pt for methanol oxidation. It is evident from Fig. 10 that PANI-PSS-Pt can be operated at a longer time than PANI-Pt at the same current density. This demonstrates that the activity and the stability of PANI-PSS-Pt were higher than PANI-Pt. The better stability for PANI-PSS-Pt might be related to the more homogeneous dispersion of Pt than PANI-Pt. Besides that, the incorporation of PSS into PANI might hinder the formation of strongly absorbed poisonous species on the Pt surface and lower the poison effect of CO species [40] (Fig. 10).

4. Conclusions

PANI doped with PSS forms a spatial network structure for the distribution of SO_3H. The spatial network structure of PANI-PSS has minimum side products with improving the electrochemical properties. The existence of SO_3H in PANI-PSS spatial structure assists holding Pt^{4+} ions in the polymer matrix, resulting the homogenous distribution of Pt in PANI-PSS even thought under negative applied potential. PANI-PSS-Pt revealed the better electrocatalytic activity and stability for methanol oxidation than PANI-Pt.

Acknowledgement

The financial support of this work by the National Science Council of Taiwan under NSC-95-221-E-006-325, NSC 95-28

11-E-006-021 and NSC 95-2211-E-006-409-MY3 is gratefully acknowledged.

References

[1] C.Y. Chen, P. Yang, Y.S. Lee, K.F. Lin, J. Power Sources 141 (2005) 24.
[2] J.B. Ge, H.T. Liu, J. Power Sources 142 (2005) 56.
[3] H.S. Liu, C.J. Song, L. Zhang, J.J. Zhang, H.J. Wang, D.P. Wilkinson, J. Power Sources 155 (2006) 95.
[4] G. Wu, L. Li, J.H. Li, B.Q. Xu, J. Power Sources 155 (2006) 118.
[5] R. Dillon, S. Srinivasan, A.S. Aricò, V. Antonucci, J. Power Sources 127 (2004) 112.
[6] M. Carmo, V.A. Paganin, J.M. Rosolen, E.R. Gonzalez, J. Power Sources 142 (2005) 169.
[7] G. Wu, Y.S. Chen, B.Q. Xu, Electrochem. Commun. 7 (2005) 1237.
[8] H.J. Wang, H. Yu, F. Peng, P. Lv, Electrochem. Commun. 8 (2006) 499.
[9] C.A. Bessel, K. Laubernds, N.M. Rodrigue, R.T.K. Baker, J. Phys. Chem. B 105 (2001) 1115.
[10] E.S. Steigerwalt, G.A. Deluga, D.E. Cliffel, C.M. Lukehart, J. Phys. Chem. B 105 (2001) 8097.
[11] Z.L. Liu, X.H. Lin, J.Y. Lee, W. Zhang, M. Han, L.M. Gan, Langmuir 18 (2002) 4054.
[12] W.Z. Li, C.H. Liang, W.J. Zhou, J.S. Qiu, Z.H. Zhou, G.Q. Sun, Q. Xin, J. Phys. Chem. B 107 (2003) 6292.
[13] Y.C. Liu, X.P. Qiu, Y.Q. Huang, W.T. Zhu, Carbon 40 (2002) 2375.
[14] Y.C. Liu, X.P. Qiu, W.T. Zhu, G.S. Wu, J. Power Sources 114 (2003) 10.
[15] B. Rajesh, K.R. Thampi, J.M. Bonard, H.J. Mathieu, N. Xanthopoulos, B. Viswanathan, J. Power Sources 141 (2005) 35.
[16] Y.M. Wu, W.S. Li, J. Lu, J.H. Du, D.S. Lu, J.M. Fu, J. Power Sources 145 (2005) 286.
[17] F.Y. Xie, Z.Q. Tian, H. Meng, P.K. Shen, J. Power Sources 141 (2005) 211.
[18] H.S. Park, Y.J. Kim, W.H. Hong, H.K. Lee, J. Membr. Sci. 272 (2006) 28.
[19] H.P. Choo, K.Y. Liew, H.F. Liu, C.E. Seng, W.A.K. Mahmood, M. Bettahar, J. Mol. Catal. A: Chem. 191 (2003) 113.
[20] S.P. Jiang, Z. Liu, H.L. Tang, M. Pan, Electrochim. Acta 51 (2006) 5721.
[21] L. Niu, Q. Li, F. Wei, S. Wu, P. Liu, X. Cao, J. Electroanal. Chem. 578 (2005) 331.
[22] L.C. Cogo, M.V. Batisti, M.A. Pereira-da-Silva, O.N. Oliveira Jr., F.C. Nart, F. Huguenin, J. Power Sources 158 (2006) 160.
[23] F. Bensebaa, A.A. Farah, D. Wang, C. Bock, X. Du, J. Kung, Y. Le Page, J. Phys. Chem. B 109 (2005) 15339.
[24] X. Jiang, L. Zhang, S. Dong, Electrochem. Commun. 8 (2006) 1137.
[25] T.C. Wen, L.M. Huang, A. Gopalan, Electrochim. Acta 46 (2001) 2463.
[26] J. Huang, J.A. Moore, J.H. Acquaye, R.B. Kaner, Macromolecules 38 (2005) 317.
[27] T.C. Wen, L.M. Huang, A. Gopalan, J. Electrochem. Soc. 148 (2001) D9.
[28] W.C. Chen, T.C. Wen, A. Gopalan, J. Electrochem. Soc. 148 (2001) E427.
[29] H. Ding, S.M. Park, J. Electrochem. Soc. 150 (2003) E33.
[30] Y. Kang, M.H. Lee, S.B. Rhee, Synth. Met. 52 (1992) 319.
[31] Y.K. Zhou, B.L. He, W.J. Zhou, H.L. Li, J. Electrochem. Soc. 151 (2004) A1052.
[32] F. Beck, Electrochim. Acta 33 (1988) 839.
[33] K. Bouzek, K.-M. Mangold, K. Jutter, Electrochim. Acta 46 (2000) 661.
[34] F. Xie, Z. Tian, H. Meng, P.K. Shen, J. Power Sources 141 (2005) 211.
[35] A. Chen, D.J.L. Russa, B. Miller, Langmuir 20 (2004) 9695.
[36] M.A.A. Rahim, R.M.A. Hameed, M.W. Khalil, J. Power Sources 135 (2004) 42.
[37] S.Q. Song, Z.X. Liang, W.J. Zhou, G.Q. Sun, Q. Xin, V. Stergiopoulos, P. Tsiakaras, J. Power Sources 145 (2005) 495.
[38] A. Dalmia, C.L. Lineken, R.F. Savinell, J. Colloid Interface Sci. 205 (1998) 535.
[39] T.S. Ahmadi, Z.L. Wang, T.C. Green, A. Henglein, M.A. Elayed, Science 272 (1996) 1924.
[40] V.E. Kazarinov, V.N. Andreev, M.A. Spitsyn, A.P. Mayorov, Electrochim. Acta 35 (1990) 1459.